nature nanotechnology

LETTERS

PUBLISHED ONLINE: 26 MAY 2013 | DOI: 10.1038/NNANO.2013.96

Voltage-controlled domain wall traps in ferromagnetic nanowires

Uwe Bauer, Satoru Emori and Geoffrey S. D. Beach*

Electrical control of magnetism has the potential to bring about revolutionary new spintronic devices[1–5], many of which rely on efficient manipulation of magnetic domain walls in ferromagnetic nanowires[2–4]. Recently, it has been shown that voltage-induced charge accumulation at a metal–oxide interface can influence domain wall motion in ultrathin metallic ferromagnets[6–8], but the effects have been relatively modest and limited to the slow, thermally activated regime[9]. Here we show that a voltage can generate non-volatile switching of magnetic properties at the nanoscale by modulating interfacial chemistry rather than charge density. Using a solid-state ionic conductor as a gate dielectric[10,11], we generate unprecedentedly strong voltage-controlled domain wall traps that function as non-volatile, electrically programmable and switchable pinning sites. Pinning strengths of at least 650 Oe can be readily achieved, enough to bring to a standstill domain walls travelling at speeds of at least ~20 m s^{-1}. We exploit this new magneto-ionic effect to demonstrate a prototype non-volatile memory device in which voltage-controlled domain wall traps facilitate electrical bit selection in a magnetic nanowire register.

Magnetic anisotropy in ultrathin metallic ferromagnets can be tuned by an electric field[12–14], opening the door to ferromagnetic field-effect devices in which a gate voltage can control the magnetic state[15–17]. Magnetoelectric coupling in metals has, until now, been achieved by charging up a ferromagnetic thin film, which acts as one plate of a capacitor. Electron accumulation or depletion of the ferromagnet can alter its magnetic properties[12–14,18], but because the charge density of a metal can be varied only slightly, the change in magnetic anisotropy energy is small and fundamentally limited. Although this mechanism was recently used to modulate domain wall velocity in nanometre-thick cobalt films[6–9], the effect could only be detected in the slow, thermally activated creep regime (μm s^{-1} to mm s^{-1}) where velocity is exponentially sensitive to surface anisotropy[9]. By contrast, practical devices require the manipulation of domain walls travelling at tens to hundreds of metres per second; so far, this has remained out of reach.

Perpendicular magnetic anisotropy (PMA) in Co/metal-oxide bilayers derives from interfacial Co–O hybridization[19], and slight changes to the interfacial oxidation state have a pronounced impact on PMA[19,20]. Here we propose that, by using a gate oxide with high ionic mobility, one can electrically displace O^{2-} at the Co–O interface[10,11,21,22] and thereby not just tune the anisotropy, but also remove and reintroduce its very source. By using an amorphous rare-earth gate oxide and providing a high-diffusivity path for ionic exchange, we show that magnetic anisotropy can be toggled at the nanoscale. We then harness this to create voltage-controlled domain wall traps with unprecedented pinning strength. Moreover, because the effect does not rely on maintaining an electrical charge, these voltage-induced changes to magnetic properties persist at zero bias, enabling non-volatile switching and state retention in the power-off state. Our work highlights a new opportunity for merging nanoionics[10,11] and nanomagnetics into novel 'magneto-ionic' devices. These are an attractive alternative to magnetoelectric composites, which rely on complex oxides (piezoelectrics or ferroelectrics) to achieve similar functionality[23–27].

We used Ta(4 nm)/Pt(3 nm)/Co(0.9 nm)/GdOx(3 nm) films with strong PMA[19,20] and an in-plane saturation field of >10 kOe (GdOx, gadolinium oxide). On those films, a second 30-nm-thick

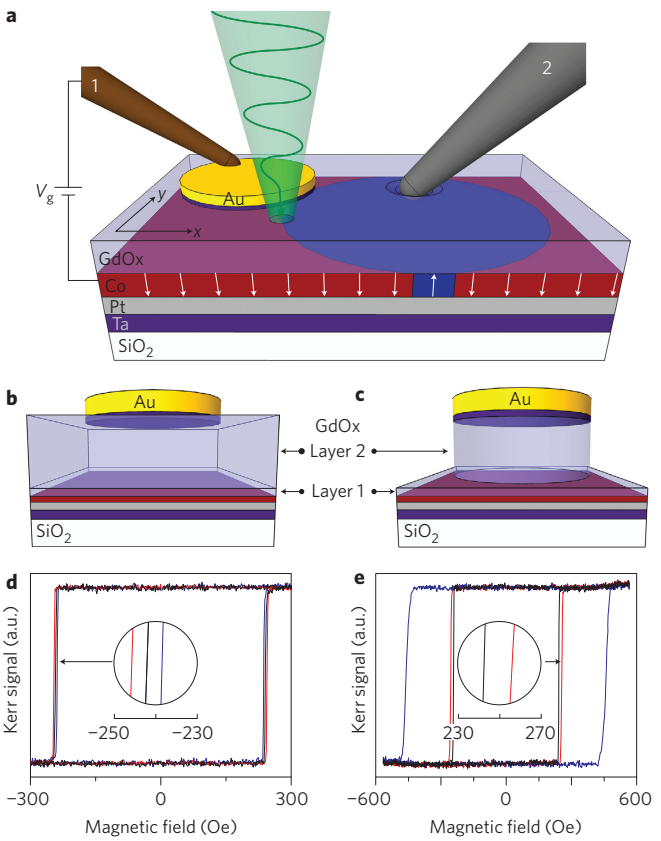

Figure 1 | Experiment schematics and magnetic hysteresis loops. **a**, Schematic showing the Ta/Pt/Co/GdOx structure, a BeCu microprobe for voltage application (1), a tungsten microprobe to create an artificial domain wall nucleation site (2), and a focused MOKE laser probe (green cone) to map out (x, y) magnetic domain expansion. **b**,**c**, Device schematic showing the double-layer GdOx dielectric with continuous second layer (sample A) (**b**) and patterned second layer (sample B) (**c**). **d**,**e**, Hysteresis loops for sample A (**d**) with $V_g = 0$ V (black line), −7 V (blue line) and +6 V (red line) and for sample B (**e**) in the virgin state (black line) and after $V_g = -6$ V for 180 s (blue line) and $V_g = +6$V for 300 s (red line). Insets: magnified section of hysteresis loops.

Department of Materials Science and Engineering, Massachusetts Institute of Technology, Cambridge, Massachusetts 02139, USA. *e-mail: gbeach@mit.edu

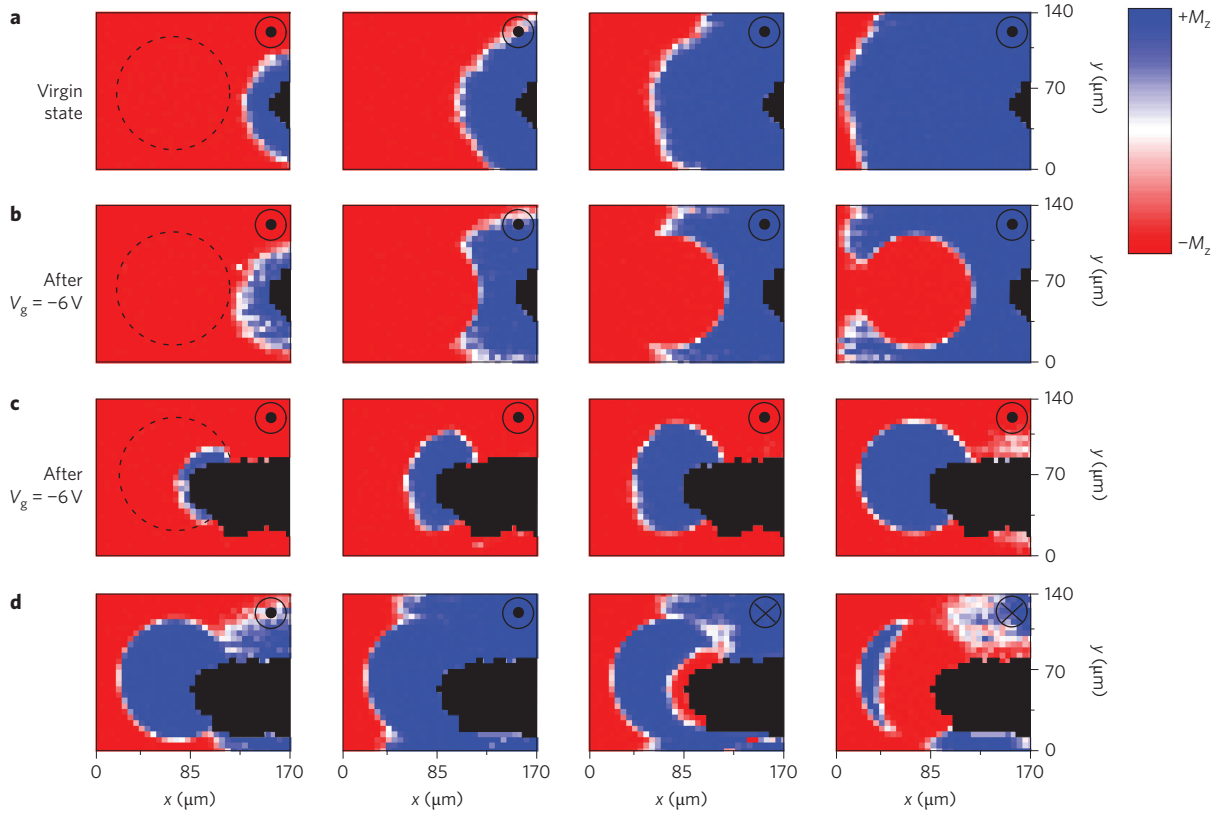

Figure 2 | Space- and time-resolved domain expansion. a–d, Sequences of polar MOKE maps showing domain expansion on sample B with increasing time (left to right) under a driving field of $H = 170$ Oe. Sequence **a** shows the virgin device state and sequences **b–d** correspond to the high-H_c state with $H_c = 460$ Oe after application of $V_g = -6$ V for 180 s. All maps (**a–d**) were measured at $V_g = 0$ V with an artificial nucleation site either outside (**a**,**b**) or inside (**c**,**d**) the electrode. Domain expansion in **d** is a continuation of **c** with the H direction reversed after the second map. Sequences **a–c** span 9.8 ms, 9.8 ms and 4.2 ms, respectively. Sequence **d** spans 12.2 ms and H was reversed after 6.2 ms. Symbols in the upper right corner of each map (**a–d**) indicate H direction. Dashed black circles in **a–c** show the outline of the gate electrode, and the black map area (**a–d**) corresponds to the tungsten microprobe used to create the artificial nucleation site.

GdOx overlayer and a Ta/Au metal gate were deposited and patterned into two different geometries. In sample A (Fig. 1b), the GdOx overlayer is continuous and the Ta/Au layer is patterned into an array of 100-μm-diameter electrodes. In sample B (Fig. 1c), the GdOx and Ta/Au layer are patterned together into such an array. The gate structure is nominally identical for these two samples, but the devices on sample B exhibit an open oxide edge around the electrode perimeter, which is not present in sample A.

The influence of a gate voltage on domain wall propagation was investigated using the technique[8,9] described schematically in Fig. 1a. A stiff tungsten microprobe was used to create an artificial domain nucleation site in the vicinity of a gate electrode by application of a local mechanical stress. A second, mechanically compliant BeCu probe was used to gently contact the electrode and apply a gate voltage V_g. Under the application of a magnetic field, a reversed domain nucleates underneath the tungsten tip and expands radially across the film. Magnetization reversal was locally probed using a scanning magneto-optical Kerr effect (MOKE) polarimeter[9]. Figure 1d shows hysteresis loops for sample A measured near the centre of a gate electrode located ~100 μm from an artificial nucleation site, with $V_g = 0$ V, +6 V and −7 V. The coercivity H_c varies linearly and reversibly with V_g at a slope of ~0.5 Oe V^{-1}, consistent with the influence of electron accumulation/depletion on domain wall creep[6–8].

The behaviour of sample B is remarkably different. Under negative gate voltage, H_c increases with time at a rate that increases with increasing $|V_g|$. In contrast to sample A, when V_g is removed the higher H_c state is retained. As seen in Fig. 1e, H_c increases by ~230 Oe after applying $V_g = -6$ V for 180 s. This change is two orders of magnitude larger and of opposite sign compared to sample A at the same V_g. Subsequent application of positive $V_g = +6$ V for 300 s returns H_c to within 10 Oe of its initial state. H_c can be cycled in this way many times and remains stable at $V_g = 0$ for at least several days.

Figure 2 presents space- and time-resolved images of domain expansion in sample B at zero V_g, which reveal the origin of the H_c enhancement. At each pixel, the magnetization was first saturated, and then a reverse field $H = +170$ Oe was applied while acquiring a time-resolved MOKE signal transient. Fifty reversal cycles were averaged at each position, from which the average trajectory of the expanding domain was reconstructed. Figure 2a–d shows a sequence of snapshots of domain expansion at increasing times after field-step application. In the virgin state (Fig. 2a), the domain wall passes unimpeded underneath the gate electrode. However, in the high-H_c state, domain expansion is blocked at the electrode edge, regardless of whether the artificial nucleation site is outside (Fig. 2b) or inside (Fig. 2c) the electrode (see also Supplementary Fig. S1).

The domain-wall creep velocity, which depends sensitively on interface anisotropy[6,9], is unchanged underneath the electrode in the high-H_c state (Supplementary Fig. S2). Accordingly, the irreversible changes that block domain wall propagation after voltage application occur only at the electrode perimeter. This indicates the formation of either a potential barrier or a potential well depending

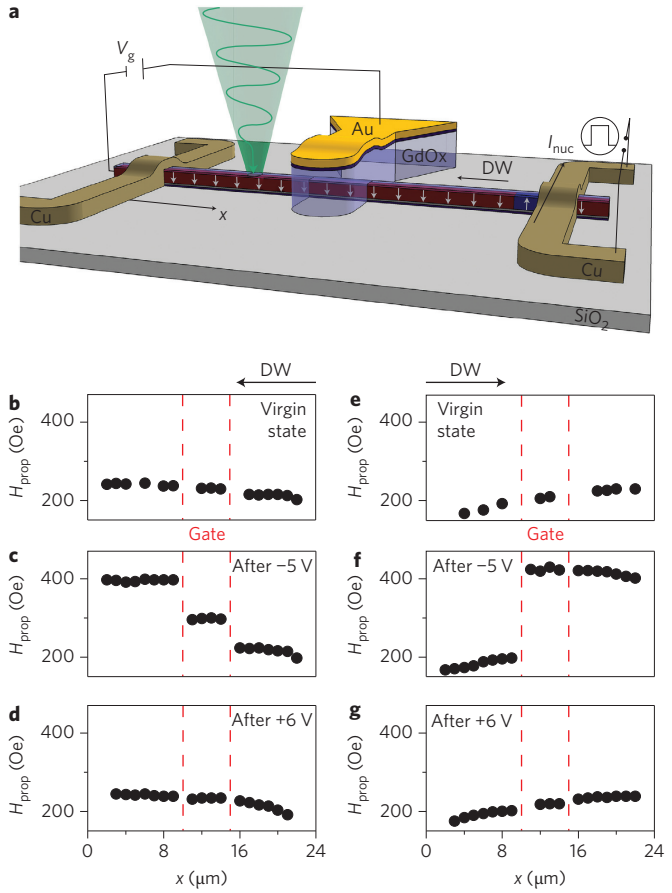

Figure 3 | Control of domain wall propagation in magnetic nanowire conduits. a, Device schematics showing a 30-μm-long and 500-nm-wide Ta/Pt/Co/GdOx nanowire conduit with orthogonal Cu lines at each end (for domain wall initialization by current pulse I_{nuc}) and a 5-μm-wide GdOx/Ta/Au gate electrode at the centre of the wire. The green cone represents a focused MOKE laser probe. **b**–**g**, Domain wall propagation field along a nanowire for the device in the virgin state (**b**,**e**), after application of $V_g = -5$ V for 60 s (**c**,**f**), and after application of $V_g = +6$ V for 120 s (**d**,**g**) with domain wall initialization from the right end (**b**–**d**) or left end (**e**–**g**) of the nanowire. All measurements at $V_g = 0$ V.

on whether the local anisotropy energy is enhanced or reduced by voltage application. The panels in Fig. 2d show a continuation of the sequence in Fig. 2c after subsequent application of a negative field step. If the electrode perimeter acted as a potential barrier, the domain within the electrode should collapse inward as the domain wall retreats from the electrode edge. However, the domain wall remains pinned at the electrode perimeter, and reversal inside the electrode instead proceeds by nucleation of a reversed domain underneath the tungsten probe tip. We therefore conclude that the electrode perimeter acts as a strong domain wall trap.

The non-volatility of this effect and its localization at the electrode perimeter, where the electrostatic field is weaker than it is at the interior, indicate that electric-field-induced electron accumulation/depletion cannot be responsible. Rather, the timescale of trap creation (seconds), together with the unprecedentedly strong influence on domain wall propagation, suggest an ionic rather than electronic origin. Rare-earth gadolinium-based oxides are well-known solid-state ionic conductors in which high O^{2-} vacancy mobility is often exploited, for example, for memristive switching devices[10,11] and oxygen exchange in solid oxide fuel cells[28]. In thin-film amorphous metal oxides, ionic exchange is particularly efficient and occurs readily at room temperature[11,21,22]. As PMA in Co/metal oxide bilayers is highly sensitive to interfacial oxygen coordination[19,20], we suggest that O^{2-} vacancy transport in the GdOx permits voltage-controlled O^{2-} accumulation or depletion near the Co/GdOx interface, which consequently alters the local magnetic energy landscape. Negative V_g is expected to drive O^{2-} towards the Co/GdOx interface, and overoxidation of the Co would decrease both PMA[19,20] and the saturation magnetization. The resulting decrease in magnetic energy density confined to a very short length scale near the electrode edge would produce a domain wall trap consistent with our observations.

Indeed, the electrode edge corresponds to the triple phase boundary (TPB) where O_2 gas, O^{2-} ion-conducting and electron-conducting phases meet and electrochemical reactions occur most efficiently[29]. Because domain wall traps are only generated near the TPB, the open oxide edge in sample B probably provides the necessary high-diffusivity path for O^{2-} ions to the Co/GdOx interface. Bulk diffusion is typically much slower than surface diffusion[30], so the timescale for these effects should be correspondingly longer for sample A, consistent with the lack of irreversibility at low voltage in that sample. Evidence of oxygen evolution near breakdown at large positive V_g, as well as photo-induced enhancement (Supplementary Figs S4, S5), further supports this conclusion.

In Fig. 3 we show that voltage-gated domain wall traps can effectively control domain wall propagation in magnetic nanowires. A 500-nm-wide, 30-μm-long Ta(4 nm)/Pt(3 nm)/Co(0.9 nm)/GdOx(3 nm) nanowire was fabricated with a 5-μm-wide GdOx(30 nm)/Ta(2 nm)/Au(12 nm) gate electrode at its centre, and domain wall nucleation lines at either end (Fig. 3a). Figure 3b–g shows the domain wall propagation field H_{prop} versus position, measured by first nucleating a domain wall at one end of the nanowire with a current pulse through the Cu line, and then sweeping H while detecting domain wall propagation using MOKE. In the virgin state (Fig. 3b,e), domain walls propagate freely underneath the gate. After applying $V_g = -5$ V for 60 s and then setting V_g to zero, H_{prop} for leftward-propagating domain walls (Fig. 3c) exhibits a large step at each edge of the gate, whereas for rightward-propagating domain walls (Fig. 3f) there is a single step at the left side of the gate. This behaviour indicates the presence of localized domain wall traps at the right and left edges of the gate, with pinning strengths of ~300 Oe and 400 Oe, respectively. As seen in Fig. 3d,g, the traps can be removed subsequently by application of a positive gate voltage.

By reducing the gate width to 800 nm (Fig. 4a), directional asymmetry in H_{prop} was greatly reduced, suggesting that the traps begin to overlap at this length scale. Figure 4b shows that H_{prop} can be programmatically set to any desired level up to at least 650 Oe (the limit of our electromagnet) by controlling the integrated voltage dwell time. At $H = 650$ Oe, domain walls travelled at ~20 m s^{-1} (Supplementary Fig. S3), and even at this speed they came to a standstill upon entering the voltage-controlled trap. In Fig. 4c, H_{prop} was repeatedly cycled between ~250 Oe and 450 Oe to demonstrate the robustness of the switching mechanism. Finally, Fig. 4d,e shows that, once set, H_{prop} remains stable at zero bias for more than 24 h.

Finally, we demonstrate an n-bit non-volatile memory cell based on $n - 1$ gate electrodes programmed as a cascaded sequence of domain wall traps with successively increasing pinning strength. An arbitrary bit sequence can then be written using a sequence of n global field pulses with successively decreasing amplitude. To write a bit pattern, a new domain wall is initialized with the injection line before each field pulse, and the pulse amplitudes are such that the mth pulse drives the initialized domain wall past the first $m - 1$ domain wall traps but not past the mth trap.

Figure 5a presents a micrograph of a three-bit register, with each bit separated by a gate electrode. Domain walls are nucleated using the Cu nucleation line to the right, and the right and left domain wall traps are set to pinning strengths of 450 Oe and 550 Oe, respectively. Three field pulses $|H| = 635$ Oe, 505 Oe and 325 Oe

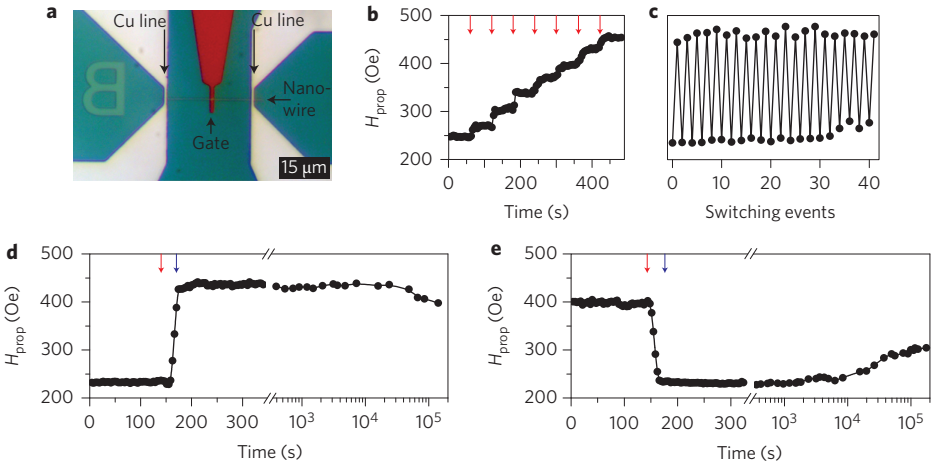

Figure 4 | Properties of domain wall traps in nanowire conduits. a, Optical micrograph showing a Ta/Pt/Co/GdOx nanowire conduit with Cu lines and a GdOx/Ta/Au gate with a reduced width of 800 nm. **b**, Stepwise increase in domain wall trap pinning strength following application of 5 s voltage pulses of $V_g = -3$ V (red arrows). **c**, Twenty switching cycles of domain wall trap pinning strength between ~250 Oe and ~450 Oe. **d**,**e**, First switching cycle of a virgin device, showing retention of pinning strength over 48 h after application of $V_g = -5$ V for 30 s (**d**) and then after $V_g = +5$ V for 30 s (**e**). Red/blue arrows in **d** and **e** indicate time of bias application/removal, respectively.

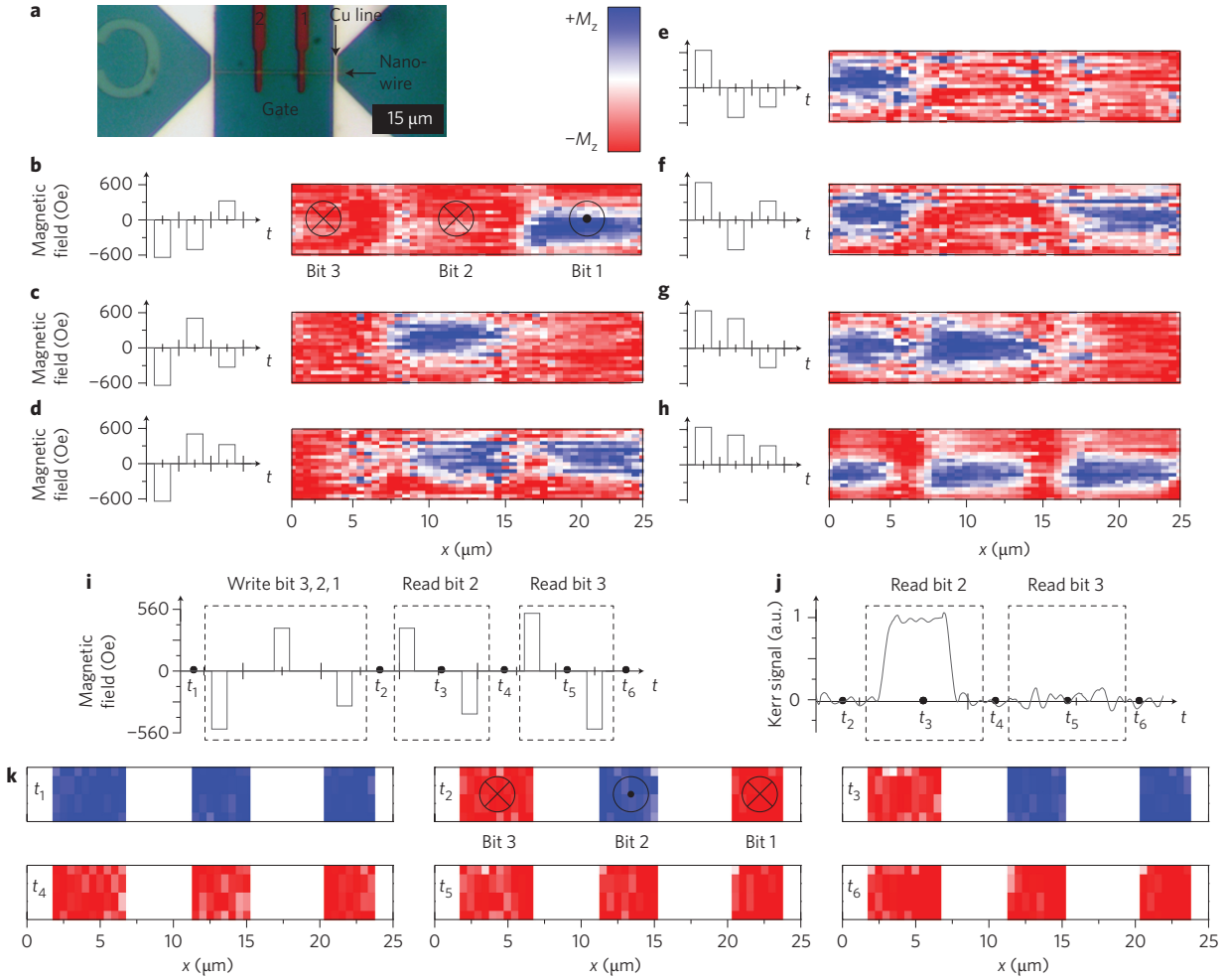

Figure 5 | Domain wall trap-based three-bit register. a, Optical micrograph showing a three-bit register consisting of a Ta/Pt/Co/GdOx nanowire conduit with Cu lines and two 800-nm-wide GdOx/Ta/Au gates. **b**–**h**, Magnetic field pulse sequence (2 ms pulse duration) and Kerr images of nanowire register in the corresponding three-bit state. **i**, Magnetic field pulse sequence (2 ms pulse duration) to write and subsequently read out the three-bit register. **j**, Kerr signal during readout of the second and third bit. **k**, Kerr images of the nanowire device at different times t_1–t_6 during the write and readout process. Symbols in the Kerr images of **b** and **k** indicate the magnetization direction of individual bits, and the white area in **k** corresponds to the area of the nanowire obstructed by the gates and Cu lines.

are used to write the three bits, with the pulse polarity determining the polarity of the corresponding bit. Field pulse sequences and MOKE maps for all possible domain states are shown in Fig. 5b–h, where the down-saturated state was used as a reference to extract the differential MOKE signal.

A complementary field pulse sequence is used to read out the bits. Here, readout is performed by MOKE with the laser spot placed on the first bit, but this could in principle be done all-electrically via a magnetic tunnel junction. For the readout process, bit 1 is read and then set to a reference state. Subsequent bits are read out in sequence by applying read and reset field pulses of equal amplitude but opposite polarity for each bit. To read the mth bit, the pulse amplitude is between the pinning strengths of the $(m-1)$th and mth domain wall traps. If the state of the mth bit is different from the reference state, the read pulse sweeps the domain wall from the $(m-1)$th domain wall trap through the first bit, where it is detected. Afterwards, the reset pulse, accompanied by a domain wall nucleation pulse, resets all previously read bits to the reference state. Otherwise the read and reset pulses have no effect. The readout process for the three-bit register is demonstrated in Fig. 5i–k, where the reference state (bit 1) is chosen to be magnetization down. An array of such devices could be driven by a single global field source, with any particular nanowire register addressed as above, while all other registers are placed in an inactive state by setting all domain wall traps to a high pinning state. Although a practical device will require significantly increasing the switching speed of the voltage-controlled traps, these results demonstrate that voltage-controlled domain wall traps can be used to realize novel devices.

In summary, we demonstrate that a functionally active gate dielectric allows the creation of voltage-controlled domain wall traps that are non-volatile, programmable and switchable. We explain the observed effects in terms of enhanced ionic mobility in the gate oxide, which permits voltage-controlled changes to interfacial ionic coordination with a consequent modification of interfacial magnetic anisotropy. The localization of this change to a narrow region at the electrode edge leads to sharp voltage-controlled magnetic potential wells with unprecedented pinning strength. Although the voltage-induced effects observed here occur over relatively long timescales, ionic transport can occur at the nanosecond timescale, as, for example, in memristive switching devices[11,31]. Optimization of the gate oxide materials and structure based on design principles that are already well established in solid-state ionic devices should permit fast voltage-induced changes to the Co–oxide interface and therefore rapid switching of magnetic properties. The merger of magnetic and solid-state ionic materials represents a novel class of functional materials that offer an alternative to traditional magnetoelectric composites based on complex oxides. By replacing ferroelectric or piezoelectric materials with simple oxide dielectrics, magneto-ionic composites could allow the realization of high-performance magnetoelectric devices using fabrication conditions compatible with complementary metal–oxide semiconductor (CMOS) processing.

Methods

Films were prepared by d.c. magnetron sputtering at room temperature under 3 mtorr argon with a background pressure of $\sim 1 \times 10^{-7}$ torr, on thermally oxidized Si(100) substrates. GdOx layers were deposited by reactive sputtering from a metal Gd target at an oxygen partial pressure of $\sim 5 \times 10^{-5}$ torr. Under these deposition conditions the GdOx layer is amorphous. Layer thicknesses were determined from the deposition rate of each material, which was calibrated by X-ray reflectivity. The magnetic properties of the Ta(4 nm)/Pt(3 nm)/Co(0.9 nm)/GdOx(3 nm) films were characterized by vibrating sample magnetometry. The films exhibited an in-plane saturation field of >10 kOe, indicating strong perpendicular magnetic anisotropy, and a saturation magnetization of ~1,200 e.m.u./(cm^3 of Co), suggesting minimal Co oxidation during growth of the GdOx overlayer.

Gate electrodes on the continuous films were patterned using electron-beam lithography and liftoff. The metal electrodes in samples A and B consisted of a Ta(2 nm)/Au(12 nm) sputter-deposited stack. The nanowire devices were fabricated using electron-beam lithography and liftoff, and were prepared in three steps (the nanowire was patterned first, followed by the Cu nucleation lines, and finally the gate electrodes were deposited). Domain walls were nucleated in these devices by the Oersted field from a 25-ns-long current pulse (~100 mA) injected through the Cu line.

Polar MOKE measurements were made using a 532 nm diode laser attenuated to 1 mW, focused to a ~3-μm-diameter probe spot and positioned by a high-resolution (50 nm) scanning stage. The Ta/Au gate electrodes were thick enough to permit robust electrical contact, but thin enough that polar MOKE measurements could be made directly through the electrodes at the 532 nm wavelength.

Magnetic hysteresis loops were measured and the domain wall propagation field was determined at a fixed sweep rate of the magnetic field of 28 kOe s^{-1}. The electromagnet used in this work had a rise time of ~300 μs, and a maximum amplitude of 650 Oe, which limited the maximum domain wall trapping potential that could be measured.

Received 11 January 2013; accepted 25 April 2013; published online 26 May 2013

References

1. Ohno, H. *et al.* Electric-field control of ferromagnetism. *Nature* **408,** 944–946 (2000).
2. Chappert, C., Fert, A. & Van Dau, F. N. The emergence of spin electronics in data storage. *Nature Mater.* **6,** 813–823 (2007).
3. Allwood, D. A. *et al.* Magnetic domain-wall logic. *Science* **309,** 1688–1692 (2005).
4. Parkin, S. S. P., Hayashi, M. & Thomas, L. Magnetic domain-wall racetrack memory. *Science* **320,** 190–194 (2008).
5. Garcia, V. *et al.* Ferroelectric control of spin polarization. *Science* **327,** 1106–1110 (2010).
6. Schellekens, A., van den Brink, A., Franken, J., Swagten, H. & Koopmans, B. Electric-field control of domain wall motion in perpendicularly magnetized materials. *Nature Commun.* **3,** 847 (2012).
7. Chiba, D. *et al.* Electric-field control of magnetic domain-wall velocity in ultrathin cobalt with perpendicular magnetization. *Nature Commun.* **3,** 888 (2012).
8. Bauer, U., Emori, S. & Beach, G. S. D. Electric field control of domain wall propagation in Pt/Co/GdOx films. *Appl. Phys. Lett.* **100,** 192408 (2012).
9. Bauer, U., Emori, S. & Beach, G. S. D. Voltage-gated modulation of domain wall creep dynamics in an ultrathin metallic ferromagnet. *Appl. Phys. Lett.* **101,** 172403 (2012).
10. Yang, J. J., Strukov, D. B. & Stewart, D. R. Memristive devices for computing. *Nature Nanotech.* **8,** 13–24 (2013).
11. Waser, R., Dittmann, R., Staikov, G. & Szot, K. Redox-based resistive switching memories—nanoionic mechanisms, prospects, and challenges. *Adv. Mater.* **21,** 2632–2663 (2009).
12. Weisheit, M. *et al.* Electric field-induced modification of magnetism in thin-film ferromagnets. *Science* **315,** 349–351 (2007).
13. Maruyama, T. *et al.* Large voltage-induced magnetic anisotropy change in a few atomic layers of iron. *Nature Nanotech.* **4,** 158–161 (2009).
14. Endo, M., Kanai, S., Ikeda, S., Matsukura, F. & Ohno, H. Electric-field effects on thickness dependent magnetic anisotropy of sputtered MgO/$Co_{40}Fe_{40}B_{20}$/Ta structures. *Appl. Phys. Lett.* **96,** 212503 (2010).
15. Wang, W. G., Li, M. G., Hageman, S. & Chien, C. L. Electric-field-assisted switching in magnetic tunnel junctions. *Nature Mater.* **11,** 64–68 (2012).
16. Shiota, Y. *et al.* Induction of coherent magnetization switching in a few atomic layers of FeCo using voltage pulses. *Nature Mater.* **11,** 39–43 (2012).
17. Bauer, U., Przybylski, M., Kirschner, J. & Beach, G. S. D. Magnetoelectric charge trap memory. *Nano Lett.* **12,** 1437–1442 (2012).
18. Chiba, D. *et al.* Electrical control of the ferromagnetic phase transition in cobalt at room temperature. *Nature Mater.* **10,** 853–856 (2011).
19. Manchon, A. *et al.* Analysis of oxygen induced anisotropy crossover in Pt/Co/MO_x trilayers. *J. Appl. Phys.* **104,** 043914 (2008).
20. Manchon, A. *et al.* X-ray analysis of the magnetic influence of oxygen in Pt/Co/AlO_x trilayers. *J. Appl. Phys.* **103,** 07A912 (2008).
21. Yang, J. J. *et al.* The mechanism of electroforming of metal oxide memristive switches. *Nanotechnology* **20,** 215201 (2009).
22. Kwon, D. H. *et al.* Atomic structure of conducting nanofilaments in TiO_2 resistive switching memory. *Nature Nanotech.* **5,** 148–153 (2010).
23. Chung, T. K., Carman, G. P. & Mohanchandra, K. P. Reversible magnetic domain-wall motion under an electric field in a magnetoelectric thin film. *Appl. Phys. Lett.* **92,** 112509 (2008).
24. Lahtinen, T. H. E., Tuomi, J. O. & van Dijken, S. Pattern transfer and electric-field-induced magnetic domain formation in multiferroic heterostructures. *Adv. Mater.* **23,** 3187–3191 (2011).
25. Dean, J., Bryan, M. T., Schrefl, T. & Allwood, D. A. Stress-based control of magnetic nanowire domain walls in artificial multiferroic systems. *J. Appl. Phys.* **109,** 023915 (2011).

26. Lahtinen, T. H. E., Franke, K. J. A. & van Dijken, S. Electric-field control of magnetic domain wall motion and local magnetization reversal. *Sci. Rep.* **2,** 258 (2012).
27. Lei, N. *et al.* Strain-controlled magnetic domain wall propagation in hybrid piezoelectric/ferromagnetic structures. *Nature Commun.* **4,** 1378 (2013).
28. Beckel, D. *et al.* Thin films for micro solid oxide fuel cells. *J. Power Sources* **173,** 325–345 (2007).
29. Mogensen, M. & Skaarup, S. Kinetic and geometric aspects of solid oxide fuel cell electrodes. *Solid State Ionics* **86–88,** 1151–1160 (1996).
30. Balluffi, R. W., Allen, S. M. & Carter, W. C. *Kinetics of Materials* 209–228 (Wiley, 2005).
31. Yang, J. J. *et al.* Memristive switching mechanism for metal/oxide/metal nanodevices. *Nature Nanotech.* **3,** 429–433 (2008).

Acknowledgements

This work was supported by the National Science Foundation (NSF-ECCS -1128439). Technical support from D. Bono, M. Tarkanian and E. Rapoport is acknowledged. The authors thank S.R. Bishop for discussions on solid oxide ion conductors. Work was performed using instruments in the MIT Nanostructures Laboratory, the Scanning Electron-Beam Lithography facility at the Research Laboratory of Electronics, and the Center for Materials Science and Engineering at MIT. S.E. acknowledges financial support from the NSF Graduate Research Fellowship Program.

Author contributions

U.B. proposed the study and G.B. supervised it. U.B. and G.B. designed the experiments with input from S.E. S.E. and U.B. prepared the samples. U.B. performed experiments on continuous film samples, and U.B. and S.E. performed experiments on nanowire samples. U.B. analysed the data and wrote the manuscript with assistance from G.B. and input from S.E. All authors discussed the results.

Additional information

Supplementary information is available in the online version of the paper. Reprints and permissions information is available online at www.nature.com/reprints. Correspondence and requests for materials should be addressed to G.S.D.B.

Competing financial interests

The authors declare no competing financial interests.